

# Structural aspects of MFTF-B integrated system tests

V.N.Karpenko

*Universities Research Association, Berkeley, Calif., USA*

T.A.Kozman

*Lawrence Berkeley Laboratory, University of California, USA*

J.Zbasnik

*Lawrence Livermore National Laboratory, Calif., USA*

## ABSTRACT

The Mirror Fusion Test Facility (MFTF-B) at Lawrence Livermore National Laboratory (LLNL) is a large, near-reactor scale experimental device intended to test an advanced plasma confinement concept in a tandem configuration [1]. The construction phase of the facility has been completed. The facility has undergone extensive system testing at the operational level without plasma. Good agreement was achieved between various analytical modeling techniques and measured structural responses.

## 1 INTRODUCTION

MFTF-B [2] has been subjected to extensive integrated system tests without plasma. Major systems were tested successfully to their operational levels [3] (see Fig. 1).

We have not been able to subject the structural systems to a combination of loads beyond normal operationing ones. Loads such as double electrical fault and earthquake loads were not simulated; yet these loads of low probability, in many cases dominated structural design requirements. The combination of extensive analysis, material properties characterization, component verification testing, integrated system testing, and quality control were employed to assure structural performance under normal and abnormal operating conditions.

## 2 STRUCTURAL CONFIGURATION

MFTF-B is composed of highly interdependent structures. The principal ones are magnet, vessel, and vault. The magnet array is made up of 42 superconducting coils, cooled by 4.5K liquid helium, that generate a magnetic field varying from 1 to 12 tesla [4] (see Fig. 2).

The vacuum vessel is a 58 m long horizontal cylinder made of 304 stainless steel, with circumferential and longitudinal stiffeners [5]. The central cell is 8 m in diameter, and the end cells are 10.8 m in diameter. The vault is a 2 m thick box-shaped structure with a central stiffening buttress. Its exterior dimensions are 73.5 m by 26 m, and it is 24.8 m high.

### 3 DESIGN AND TESTING APPROACH

Fusion devices are highly interactive structures that are subjected to a variety of structural loads, thereby requiring extensive computer modeling and simulation [6]. The abnormal loads that dictate design of most of the structural elements are the result of so-called magnetic double fault loads combined with seismic events. This set of loads is difficult, if not impossible, to stimulate physically. It was therefore necessary to develop a strategy that assured structural performance with a high confidence level for the low probability events.

The strategy of MFTF structural design consisted of several steps: 1) Integrated structural analysis with sufficient redundancy to verify modeling results. 2) Development and characterization of the material properties appropriate for the intended end use. 3) Component and subsystem tests. 4) Quality assurance program that encompasses analysis, design, fabrication, and testing. 5) Integrated system tests.

### 4 SUBSYSTEM AND COMPONENT TESTING

Components that are critical from the stand point of safety, facility performance, or impact on the structural design were tested whenever practicable. For example:

All major load carrying members (magnet hangers and devices) were tested to 150% of the predicted loads.

Extensive testing of magnet conductor packs was done to assure proper input for the structural modeling.

The vacuum vessel sections were individually vacuum tested and then retested as a complete assembly.

A series of dynamic excitations was applied to the end section of the vessel installed on the the reinforced concrete piers and housing the yin-yang magnet. The structural response was measured at different locations [7]. The frequency and damping values were then extracted for each mode shape by Fourier transform techniques. The average computed damping value was ~5% which was employed in structural analysis.

### 5 INTEGRATED SYSTEM TESTS

The main objective of the integrated system testing was to demonstrate overall machine capability. The integrated system test of MFTF encompassed combinations of the following loads: gravity, vacuum, thermal, and magnetic. As was stated before, seismic and magnetic fault loads were not simulated. To measure structural response of the system, to the operational environment 384 strain gages and 350 temperature gages were employed. The data are too voluminous to present it all in this paper. We have selected the most complex set of magnets and loading conditions to illustrate test results.

### 6 MAGNET STRUT LOADS AND CASE STRESSES

The magnets and support system were instrumented with 153 strain gages to confirm the accuracy of the loads and stress analyses and to determine peak strain levels in the magnet cases. Two linear strain gages were used on the hangers, struts, and links so that bending strains could be eliminated. Because it was necessary to rezero the strain

gage outputs before each magnet run, the gages on struts and hangers determined only magnetic loads (including kick loads), and the ones on the coil cases determined stresses due to magnetic loading.

### 6.1 Struts and hangers

Selected magnet support struts were instrumented to measure the electromagnetic loads imposed on the coils during the test operation. The load measurements were approximate because all struts were not instrumented and certain non-symmetric and moment effects could not be measured. Gages were installed on the following axial support struts and axial links between coils to measure the largest axial forces between the magnets: EMI-VESSEL, WMI-VESSEL, EMI-ET2, WS6-VESSEL, WS4-WS5.

### 6.2 Axial loads

Table 1 presents the results of the strain gage readings on the struts and links due to axial magnetic forces. The expected loads were calculated using the unit axial force matrix and the actual coil currents. Good agreement with expected values are obtained, as the measured total axial loads are within approximately 10% of the theoretical values. Because the measured strains in the WS4-WS5 links were very small, we expect the uncertainty in these measurements to be large.

The largest discrepancy in Table 1 concerns the M1 drag struts. The average values of the readings on each end agree with the expected value to within approximately 10%, which indicates that the measured axial force is within 10% of the expected value. The large differences in observed load in the two drag struts on each end imply that the yin yangs are subjected to unexpected kick loads. The kick loads are most likely due to interactions between the major radius lobes of M1 and the overlapping T2 coil. This tensile kick load is well within the capabilities of the strut.

Table 1. Comparison of expected and observed loads in struts and links due to axial forces (tension is positive; loads are in Kips).

Element	Expected Load	Observed Load	
EMI Drag Strut	325	298 (a)	(a) The difference in observed loads for the two EMI drag struts is due to a kick load between EMI and ET2.
EMI Drag Strut	325	418 (a)	
WMI Drag Strut	327	245 (b)	(b) The difference in observed loads for the two WMI drag struts is due to a kick load between WMI and WT2.
WMI Drag Strut	327	457 (b)	
EMI-ET2 Link	-137	-120	
EMI-ET2 Link	-137	-149	
WS6 Drag Strut	510	561	
WS6 Drag Strut	510	569	
WS4-WS5 Link	65	27	
WS4-WS5 Link	65	27	

### 6.3 Kick loads in hangers and lateral struts

Gages were installed on selected hanger and support struts to measure the magnetic "kick" loads caused by coil misalignment. These effects were estimated during the design phase by calculating magnet forces due to probable "maximum" coil misalignments. Table 2 presents a comparison of the observed and design kick loads. With the exception of the WT1 hanger and WT2 hanger and lateral struts, the observed kick loads are considerably less than the design values. For the WT1 and WT2 hangers, the loads are compressive and merely tend to unload the gravity load. The margin of safety is thus not degraded. For the WT2 lateral strut, the higher-than-expected tensile load reduces the margin of safety in this strut from 0.26 to 0.08. This positive margin of safety allows the struts to handle the additional loads due to trim coil operation.

Table 2. Kick loads in hangers and lateral struts (Kips).

Element	Observed Load	Design Load	Element	Observed Load	Design Load
ET2 Hanger	0	+34.2	WS1 Hanger	4	+23.5
ET2 Lateral	21	+33.3	WS1 Lateral	0	+47.1
ET1 Hanger	-13	+50.5	WS3 Hanger	-3	+23.5
ET1 Lateral	8	+57.2	WS3 Lateral	-3	+47.1
EA20 Hanger	0	+47.3	WS6 Hanger	31	+43.9
EA20 Lateral	-3	+94.5	WS6 Lateral	-33	+87.7
EAl Hanger	0	+23.2	WAl Hanger	-6	+23.2
EAl Lateral	1	+46.3	WAl Lateral	0	+46.3
ES6 Hanger	25	+43.9	WA20 Hanger	-11	+47.3
ES6 Lateral	38	+87.7	WA20 Lateral	9	+94.5
ES4 Hanger	7	+23.5	WT1 Hanger	-55	+50.5
ES4 Lateral	12	+47.1	WT1 Lateral	21	+57.2
ES2 Hanger	-15	+23.5	WT2 Hanger	-102	+34.2
ES2 Lateral	-11	+47.1	WT2 Lateral	57	+33.3

### 6.4 East yin-yang case stresses

Rectangular strain rosettes were mounted at 8 locations on EM1 and EM2: at the center of each of the 4 minor arcs and a point 70° away from the center of each minor arc where analyses predicted the highest stresses. The latter gage is in a weld region between plates of different thickness. Table 3 shows comparison.

The highest measured stress values were found to occur in the center of the minor arcs for EM2. The stresses in the EM2 minor radius are higher than for EM1 because the EM2 has to react a larger major radius lobe-spreading force. Experimentally, the ratio of the principal stress values, for EM2 to that for EM1 was found to be 1.12, which is very good agreement with the measured current ratio, 1.16.

At the center of the minor radius for EM2, we have calculated that the principal stresses should be 61 ksi hoop and -37 ksi transverse. These values compare with measured values of 74 ksi and -41 ksi listed in Table 3. This agreement is reasonable considering the fact that both longitudinal and transverse stresses have significant gradients in the vicinity of the strain gages (~5 ksi/in).

Table 3. Measured principal stresses for the east Yin Yang (ksi).

Rosette Location	Measured Values			Expected Values		
	$\sigma_P$	$\sigma_Q$	$\tau$	$\sigma_P$	$\sigma_Q$	$\tau$
EM2 Upper Small Radius (a)	74	-41	57	61	-37	49
EM2 Lower Small Radius (a)	72	-39	55	61	-37	49
EM1 Upper Small Radius (b)	66	-25	45	52	-32	41
EM1 Lower Small Radius (b)	64	-27	46	52	-32	41
EM2 Upper Butt Weld (c)	70	-15	42	69+8	7	26
EM2 Lower Butt Weld (c)	65	-18	42	69+8	7	26
EM1 Upper Butt Weld (b)	66	-14	40	59+8	6	23

For the EM2 butt weld area, we predicted a hoop stress value of 78 ksi and a transverse stress of 7 ksi for the inner surface of the small radius. The measured stress values around the corner from the predicted stress location were 67 ksi hoop and -17 ksi transverse. There was reasonable agreement considering the differences between the prediction and measurement locations and the fact that the strain gage was installed on a chamfer where stress predictions are difficult.

Although the peak measured yin-yang stresses are higher than predictions, this represents an acceptable encroachment into the safety margins in light of the measurement and prediction tolerance and the allowable effects of local stress concentrations. Although the measured shear stresses are quite high, the nature of the high, transverse stresses (caused by curved beam effects) is such that any plasticity will relieve the transverse bending stress and reduce the maximum shear stress.

### 6.5 ET2 case stresses

The ET2 coil case was instrumented with 10 rectangular strain rosettes and 10 linear strain gages. The gages were located at the symmetry plane of the minor radius, the major radius tie plates, inner chamfer areas, and areas on the case near the tie plates.

Table 4 presents the results of the measurements made during the test mode, in which the actual T2 coil current was 5328 A (85% of design). This table presents principal stresses and maximum shear stresses. The readings were corrected for magnetoresistance effects. These design values are for the operational mode, in which the T2 current was assumed to be 6278 A.

Our measurements result in a 740-kip tensile load on each of the two inner tie plates and a 560-kip tensile load on each of the two outer tie plates. Experimentally, the inner tie strap carries 57% of the total strap load. This is in excellent agreement with the prediction that the inner strap should carry 59% of the total strap load.

The experimental minor radius lobe-spreading force can be estimated by using analytical result that 83% of the spreading force is carried by the tie straps. The total experimental tie strap load is 2600 kip, which then implies a total lobe-spreading force of 3130 kip. The ratio of this experimental lobe spreading to the value predicted for higher load operating mode (4100 kip) is 0.76. This value is close to the

Table 4. ET2 case stresses (units are ksi; tension is positive)

Type	Location	Measured Values <sup>a</sup>			Design Values <sup>b</sup>		
		$\sigma_P$	$\sigma_Q$	$\tau$	$\sigma_P$	$\sigma_Q$	$\tau$
1 (Rosette)	Coil form wall	Not working			15.9	2.2	6.8
2 (Rosette)	Coil form wall	14.7	6.2	4.2	12.0	-2.0	7.0
3 (Rosette)	Coil form wall	16.5	8.7	3.9	5.0	-9.2	7.1
4 (Linear)	Coil form flange	-3.0	-	-	5.6	-	-
5 (Rosette)	Coil form flange	-9.5	0.7	5.1	-9.0	.95	5.0
6 (Rosette)	Coil form flange	-10.4	5.4	7.9	-8.5	.95	4.7
7 (Rosette)	Case wall	-12.1	0.6	6.4	-10.5	2.5	6.5
8 (Rosette)	Case wall	-12.6	-5.9	3.3	-5.5	-1.0	3.2
9 (Linear)	Case flange	1.1	-	-	7.4	-	-
10 (Rosette)	Case flange	-15.3	6.8	11.1	-24.5	-9.23	3.8
11 (Rosette)	Case flange	-11.35	3.3	7.3	-18.5	-5.79	5.3
12 (Linear)	Coil form flange	25.5	-	-	21.6	-	-
13 (Linear)	Coil form flange	Not working			22.8	-	-
14 (Linear)	Coil form flange	-2.1	-	-	2.4	-	-
15 (Linear)	Coil form flange	-5.2	-	-	3.6	-	-
16 (Linear)	Inner tie plate	43.7	-	-	66.6	-	-
17 (Linear)	Inner tie plate	30.3	-	-	40.8	-	-
18 (Linear)	Outer tie plate	32.8	-	-	43.2	-	-
19 (Linear)	Outer tie plate	22.5	-	-	25.8	-	-
20 (Rosette)	Helium vent area	-12.1	0.6	6.4	-11.4	-0.5	5.4

<sup>a</sup>Values are for operation,  $I_{T2} = 5328A$ . <sup>b</sup>Values are for  $I_{T2} = 6278A$

square of the ratio of currents (0.72), which implies that the minor radius lobe-spreading magnetic forces are mainly due to self-field. This 0.76 ratio can be used to scale the predicted tie plate, and major radius case stresses. To compare minor radius stresses however, a ratio of .85 (i.e., 5328/6278) is more appropriate because the major radius lobe spreading forces (which drive the minor radius stresses) are due primarily to the interaction with the M1 coil which has the same current at various operating modes. In general, the experimental case stresses exceeded the design values. This may be caused by the suspected interference between EM1 and ET2 when the coils are energized. In any case, although these observed stresses exceeded the design values, they are still well within the design guidelines and provide a generous margin of safety. The stresses in the areas of load transfer into the tie straps (rosettes 10 and 11), are about 83% of the scaled-down (84.76) design values.

### 6.6 ET1 case stresses

The ET1 coil case was fitted with 9 rectangular strain rosettes (45° petals) and 4 linear strain gages. Five rosettes (gages 1-5) are located around the case structure on the minor radius symmetry plane, four rosettes (gages 8-11) are located on the major radius symmetry plane, and around the main helium vent two, linear gages (gages 6A and 7B) are arranged to measure hoop stress, while the remaining two linear gages (gages 6B and 7A) measure transverse stress.

Table 5 presents the experimentally determined principal and maximum shear stresses for the ETL coil. These values were computed from the strains, while the ETL current was at 4661 A. Also presented on this table are design values for the operational mode, in which coil current is assumed to be 5258 A.

Fair agreement can be observed between the measured values and the expected values, which are assumed to be the design values, scaled by the square of ratio of current (0.79). This scaling law was found to be approximately correct for the T2 coil minor radius spreading forces. The experimentally determined stresses in the minor radius symmetry plane (gages 1-5) were generally lower than the expected values by up to 3 ksi. On the other hand, the measured stresses in the major radius symmetry plane were generally higher than the expected values by up to 8 ksi on the tension side and agreed within 1 ksi on the compression side. Stresses around the helium vent were approximately 50% of the expected values because finite element model overpredicted the effects of the vent cutout.

The reasons for these discrepancies is measurement accuracy at very low test stresses, but in all instances the observed stresses are all well within the design allowable.

Table 5. ETL case stresses (units are ksi; tension is positive).

Type	Location	Measured <sup>a</sup>			Design <sup>b</sup>		
		$\sigma_P$	$\sigma_Q$	$\tau$	$\sigma_P$	$\sigma_Q$	$\tau$
1 (Rosette)	Case wall	-11.5	5.0	8.2	-14.4	-0.7	6.8
2 (Rosette)	Case flange	-6.7	0.5	3.6	-9.9	0.3	5.1
3 (Rosette)	Case flange	8.9	0.2	4.4	14.2	4.6	4.8
4 (Rosette)	Coil form wall	23.3	-4.0	13.6	22.6	6.5	8.1
5 (Rosette)	Coil form flange	Not working			8.1	-2.6	5.3
6A(Linear)	Helium vent area	-9.2	-	-	-21.6	-	-
6B(Linear)	Helium vent area	-1.6	-	-	Not available		
7A(Linear)	Helium vent area	-2.4	-	-	Not available		
7B(Linear)	Helium vent area	-4.9	-	-	-12.1	-	-
8 (Rosette)	Coil form flange	21.4	-1.6	11.5	17.9	-1.2	9.6
9 (Rosette)	Coil form flange	20.5	9.96	5.3	7.8	-17.2	12.5
10 (Rosette)	Coil form flange	18.9	-0.2	9.6	14.8	-4.7	9.8
11 (Rosette)	Coil form flange	-17.5	3.9	10.7	-23.4	-11.4	6.0

<sup>a</sup>Values are for operation at  $I_{T1}=4661$  A. <sup>b</sup>Values are for  $I_{T1}=5258$  A.

## 6.7 Solenoid coil stresses

The limit on the length of the paper does not permit detailed discussion of the test results. The measured stresses were generally low and agree well with analytical predictions.

## 7 RESULTS AND CONCLUSIONS

Generally good agreement was achieved between various analytical modeling techniques and the measured structural response with only minor

exceptions from a structural point of view. The yin yang measured stresses were consistently within 20% of calculated values. We believe this is good for the very complex structure subjected to high and complex loading. The ET2 stresses data is also within 20% on the tie plates. It was particularly gratifying to observe that misalignment loads, which depend on quality of assembly and fabrication, were kept within predicted limits. MFTF operational capability, within the limits of the test configuration, was demonstrated. The analytical tools employed proved adequate to design and predict structural behavior of the MFTF system.

#### ACKNOWLEDGMENTS

The authors wish to acknowledge the contribution toward design, analysis and fabrication of the magnets by General Dynamics and the vessel by Pittsburgh-Des Moines Corporation.

Operated by Universities Research Association for the U.S. Department of Energy.

#### REFERENCES

1. Thomassen, K.I. and V.N. Karpenko 1982. An axicell design for the end plugs of MFTF-B. Lawrence Livermore National Laboratory, Livermore, CA. UCID-19318.
2. Karpenko, V.N. 1983. The mirror fusion test facility: an intermediate device of a mirror fusion reactor. Lawrence Livermore National Laboratory, Livermore, CA. UCRL-88950.
3. Krause, K.H. and T.A. Kozman, et al. 1986. MFTF-B pace tests and final cost report. Lawrence Livermore National Laboratory, Livermore, CA. UCID-20819.
4. Kozman, T., D. Shimer, J. VanSant and J. Zbasnik 1986. Construction and testing of the mirror fusion facility magnets. Lawrence Berkeley Laboratory, Berkeley, CA. LBL-21798.
5. Gerich, J.W. 1986. The vacuum vessel for the tandem mirror fusion test facility. Lawrence Livermore National Laboratory, Livermore, CA. UCRL-53701.
6. Karpenko, V.N. and D.S. Ng 1985. Application of structural-mechanics methods to the design of large tandem-mirror fusion devices (MFTF-B). Lawrence Livermore National Laboratory, Livermore, CA. UCRL-92246.
7. Weaver, H.J. et al. 1982. Dynamic testing of MFTF containment vessel structural system. Lawrence Livermore National Laboratory, Livermore, CA. UCRL-53307.

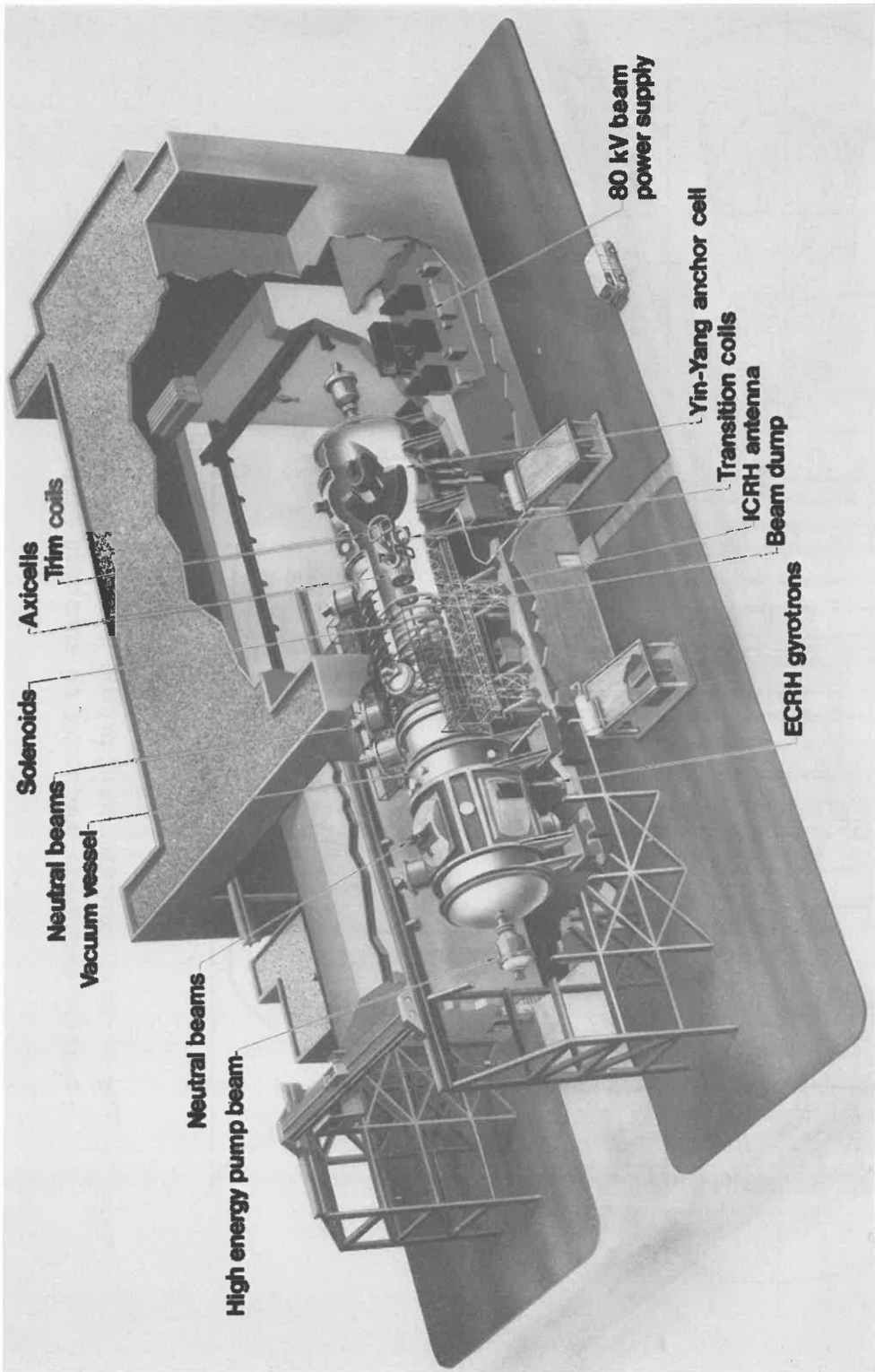


Figure 1. MFIT-B.

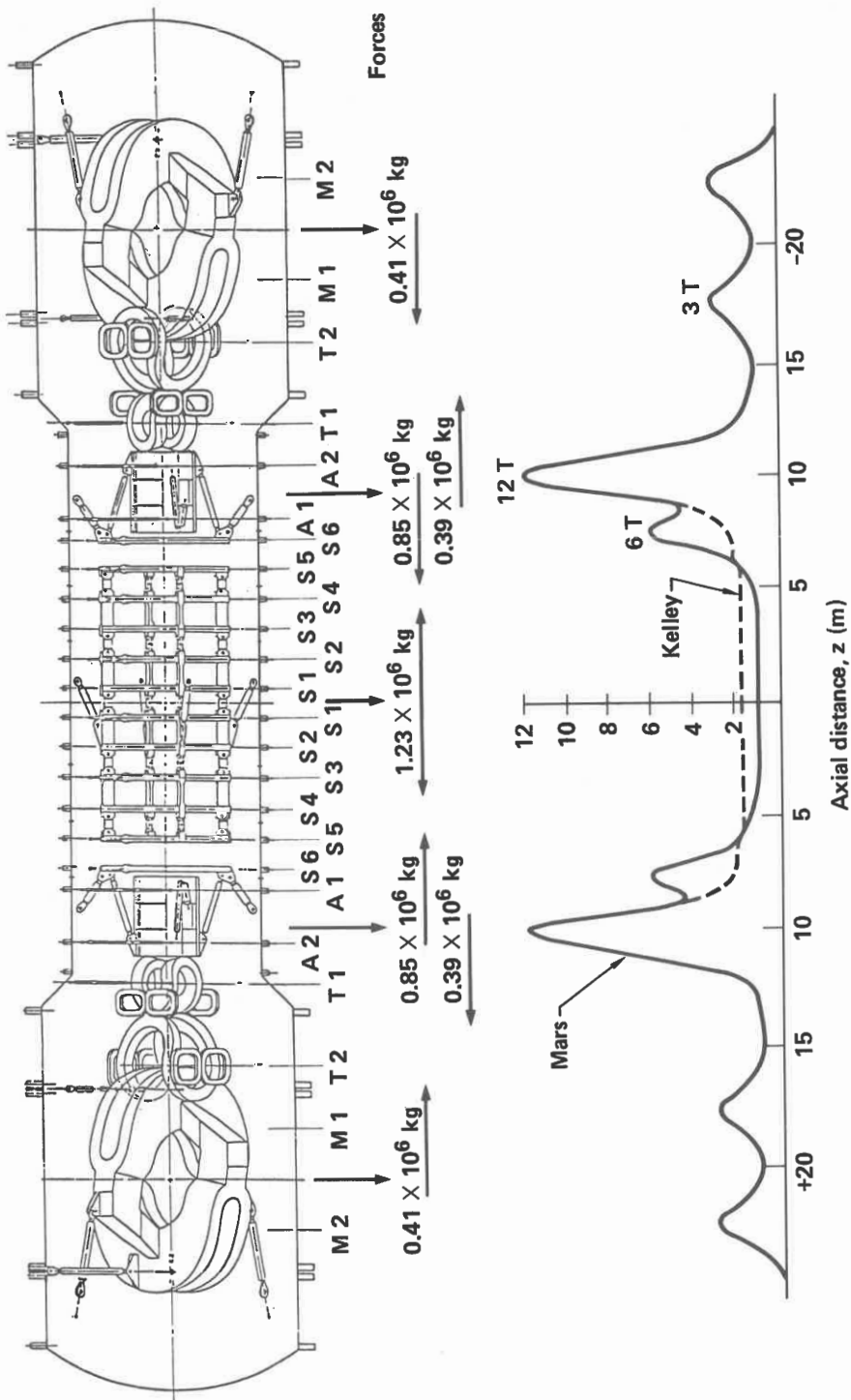


Figure 2. The on-axis magnetic field profile showing two operating modes: Mars a reactor-like mode, and Kelly an enhanced neutron-production mode.